ACADEMIC PRESS

Available online at www.sciencedirect.com

SCIENCE DIRECT®

Journal of Sound and Vibration 260 (2003) 589–609

JOURNAL OF SOUND AND VIBRATION

www.elsevier.com/locate/jsvi

Modal voltages and micro-signal analysis of conical shells of revolution

H.S. Tzou*, W.K. Chai, D.W. Wang

Structronics Labaratory, Department of Mechanical Engineering, University of Kentucky, Lexington, KY 40506-0108, USA

Received 29 January 2001; accepted 28 April 2002

Abstract

Conical shells and components are widely used as nozzles, injectors, rocket fairings, turbine blades, etc. Dynamic and vibration characteristics of conical shells have been investigated over the years. In this paper, micro-electromechanics and distributed sensing phenomena of a generic double-curvature shell and a conical shell are discussed, and governing sensing signal-displacement equations are derived. Spatially distributed modal voltages and micro-signal generations of conical shells laminated with distributed piezoelectric sensor layers are investigated based on the Donnel–Mushtari–Valsov theory. Distributed modal voltages and their various signal components of two conical shells reveal that the dominating signal component among the four contributing micro-signal components is the circumferential membrane component. This dominance is even more significant for lower shell modes and/or deep shells. In general, high strain regions result in high signal magnitudes. Accordingly, the spatially distributed signal patterns—*the modal voltages*—clearly represent the modal dynamic and micro-strain characteristics of conical shells.

1. Introduction

Jet nozzles, injectors, blades, rocket fairings, etc. in turbomachinery, aerospace structures, micro-electromechanical systems, etc. are often made of conical shell structures and components. Dynamics and vibrations of conical shell structures have been investigated over the years [1–10]. However, distributed sensing and control of conical shells have not been thoroughly investigated [11]. This study is to investigate the dynamic sensing characteristics, micro-signal generations, and distributed modal voltages of truncated conical shell sections.

*Corresponding author. Tel.: +1-606-257-2766; fax: +1-606-257-3304.
E-mail address: hstzou@engr.uky.edu (H.S. Tzou).

0022-460X/03/$ - see front matter
doi:10.1016/S0022-460X(02)00956-2

Recent development in smart structures and structronic systems has explored many new measurement and control techniques using smart materials [12,13]. Among the popular smart materials (e.g., piezoelectrics, electro- and magneto-strictive materials, shape memory materials, photostrictive materials, pyroelectric materials, electro- and magneto-rheological fluid, etc.), piezoelectric materials provide bi-directional sensing and control capability and thus it becomes one of the best candidates in both distributed sensing and control applications. Unlike conventional discrete sensors, thin piezoelectric layers can be spatially spread and distributed over the surfaces of shells and plates. Accordingly, these distributed piezoelectric layers can serve as distributed neurons and actuators in sensing and control of shells and plates [14,15].

Spatially distributed sensing signal generations of a distributed piezoelectric sensor layer laminated on a generic double-curvature elastic shell are discussed first. The generic sensing signal equation is derived based on the direct piezoelectric effect, the Gauss theory, the open-circuit assumption, the Maxwell equation, and also the generic double-curvature thin shell theory. Detailed micro-electromechanical characteristics resulting from various meridional and circumferential membrane/bending strain components are evaluated and applied to conical shells. Final closed-form sensing signal of distributed conical shell sensors is then defined based on given boundary conditions and mode shape functions in the Donnel–Mushtari–Valsov theory. Spatially distributed modal voltages, micro-signal components and modal sensing signals in both longitudinal and circumferential directions of two conical shells are thoroughly evaluated in case studies.

2. Generic shell sensing equation

It is assumed that a distributed piezoelectric sensor layer is laminated on a double-curvature generic elastic shell. The distributed sensing layer generates electrical signals, resulting from shell micro-strain variations, and the signal amplitude ϕ^s is a function of piezoelectric (displacement) constant h_{ij} and induced strains S_{ij}^S in the sensor layer [15],

$$\phi^s = \frac{h^s}{S^e}\int_{\alpha_1}\int_{\alpha_2}\left(h_{31}S_{11}^s + h_{32}S_{22}^s + h_{36}S_{12}^s\right)A_1A_2\,\mathrm{d}\alpha_1\,\mathrm{d}\alpha_2, \tag{1}$$

where the superscript 's' denotes the distributed sensor layer, h^s is the sensor thickness, S^e is the surface area of the sensor layer, α_1 and α_2 are the two principle directions in the generic shell continuum, A_1 and A_2 are the Lamé parameters, h_{31}, h_{32} and h_{36} are the piezoelectric (displacement) constants. Note that the generic sensing signal equation is derived based on the direct piezoelectric effect, the Gauss theory, the open-circuit assumption, the Maxwell equation, and also the generic double-curvature thin shell theory [16]. The effects of transverse shear and normal strains (i.e., S_{13}, S_{23} and S_{33}) are neglected. This is due to the deformation variation is small in the α_3 direction, provided the shell structures is thin. Moreover, the strain terms in the sensing equation consist of the membrane strain and the bending strain components:

$$S_{11}^s = s_{11}^o + r_1^s k_{11}, \qquad S_{22}^s = s_{22}^o + r_2^s k_{22}, \qquad S_{12}^s = s_{12}^o + r_{12}^s k_{12}, \tag{2-4}$$

where r_1^s, r_2^s, and r_{12}^s denote the sensor location away from the neutral surface of the shell and $r_1^s = r_2^s = r_{12}^s$ for shell and sensor layer with uniform thickness. The k_{ij} terms combined with r_1^s, r_2^s, and r_{12}^s denote the bending strains; s_{ij}^o denotes the membrane strains. (Note that the strains are

denoted $s_{11}^o \equiv s_1^o$, $s_{22}^o \equiv s_2^o$, $s_{12}^o \equiv s_6^o$, $k_{11} \equiv k_1$, $k_{22} \equiv k_2$ and $k_{12} \equiv k_6$ for simplicity.) Detailed membrane and bending strains (s_i^o and k_i) in the sensor layer bonded on a non-linear shell with the von-Karmon geometric non-linearity are expressed as functions of displacements—u_i's, the Lamé parameters (A_1 and A_2), and two radii of curvature (R_1 and R_2) [17].

$$s_1^o = \frac{1}{A_1}\frac{\partial u_1}{\partial \alpha_1} + \frac{u_2}{A_1 A_2}\frac{\partial A_1}{\partial \alpha_2} + \frac{u_3}{R_1} + \frac{1}{2}\left(\frac{\partial u_3/\partial \alpha_1}{A_1}\right)^2, \tag{5}$$

$$s_2^o = \frac{1}{A_2}\frac{\partial u_2}{\partial \alpha_2} + \frac{u_1}{A_1 A_2}\frac{\partial A_2}{\partial \alpha_1} + \frac{u_3}{R_2} + \frac{1}{2}\left(\frac{\partial u_3/\partial \alpha_2}{A_2}\right)^2, \tag{6}$$

$$s_6^o = \frac{1}{A_2}\frac{\partial u_1}{\partial \alpha_2} + \frac{1}{A_1}\frac{\partial u_2}{\partial \alpha_1} - \frac{u_1}{A_1 A_2}\frac{\partial A_1}{\partial \alpha_2} - \frac{u_2}{A_1 A_2}\frac{\partial A_2}{\partial \alpha_1} + \left(\frac{1}{A_1 A_2}\frac{\partial u_3}{\partial \alpha_1}\frac{\partial u_3}{\partial \alpha_2}\right), \tag{7}$$

$$k_1 = \frac{1}{A_1}\frac{\partial}{\partial \alpha_1}\left(\frac{u_1}{R_1} - \frac{1}{A_1}\frac{\partial u_3}{\partial \alpha_1}\right) + \frac{1}{A_1 A_2}\left(\frac{u_2}{R_2} - \frac{1}{A_2}\frac{\partial u_3}{\partial \alpha_2}\right)\frac{\partial A_1}{\partial \alpha_2}, \tag{8}$$

$$k_2 = \frac{1}{A_2}\frac{\partial}{\partial \alpha_2}\left(\frac{u_2}{R_2} - \frac{1}{A_2}\frac{\partial u_3}{\partial \alpha_2}\right) + \frac{1}{A_1 A_2}\left(\frac{u_1}{R_1} - \frac{1}{A_1}\frac{\partial u_3}{\partial \alpha_1}\right)\frac{\partial A_2}{\partial \alpha_1}, \tag{9}$$

$$\begin{aligned} k_6 = {} & \frac{1}{A_2}\frac{\partial}{\partial \alpha_2}\left(\frac{u_1}{R_1} - \frac{1}{A_1}\frac{\partial u_3}{\partial \alpha_1}\right) + \frac{1}{A_1}\frac{\partial}{\partial \alpha_1}\left(\frac{u_2}{R_2} - \frac{1}{A_2}\frac{\partial u_3}{\partial \alpha_2}\right) \\ & - \frac{1}{A_1 A_2}\left(\frac{u_1}{R_1} - \frac{1}{A_1}\frac{\partial u_3}{\partial \alpha_1}\right)\frac{\partial A_1}{\partial \alpha_2} - \frac{1}{A_1 A_2}\left(\frac{u_2}{R_2} - \frac{1}{A_2}\frac{\partial u_3}{\partial \alpha_2}\right)\frac{\partial A_2}{\partial \alpha_1}. \end{aligned} \tag{10}$$

Note that the quadratic terms (non-linear terms) inside the brackets of membrane strains are contributed by the large deflection, which are neglected in linear shells. Substituting the linear strain–displacement relations, Eqs. (5)–(10), into the generic signal equation, Eq. (1), yields the signal-displacement equation of a generic distributed shell sensor [14]:

$$\begin{aligned} \phi^s = {} & \left(\frac{h^s}{S^e}\right)\int_{\alpha_1}\int_{\alpha_2}\left\{h_{31}\left\{\frac{1}{A_1}\left(\frac{\partial u_1}{\partial \alpha_1} + \frac{u_2}{A_1 A_2}\frac{\partial A_1}{\partial \alpha_2} + \frac{u_3}{R_1}\right)\right.\right. \\ & \left. + r_1^s\left[\frac{1}{A_1}\frac{\partial}{\partial \alpha_1}\left(\frac{u_1}{R_1} - \frac{1}{A_1}\frac{\partial u_3}{\partial \alpha_1}\right) + \frac{1}{A_1 A_2}\left(\frac{u_2}{R_2} - \frac{1}{A_2}\frac{\partial u_3}{\partial \alpha_2}\right)\frac{\partial A_1}{\partial \alpha_2}\right]\right\} \\ & + h_{32}\left\{\frac{1}{A_2}\left(\frac{\partial u_2}{\partial \alpha_2} + \frac{u_1}{A_1 A_2}\frac{\partial A_2}{\partial \alpha_1} + \frac{u_3}{R_2}\right)\right. \\ & \left. + r_2^s\left[\frac{1}{A_2}\frac{\partial}{\partial \alpha_2}\left(\frac{u_2}{R_2} - \frac{1}{A_2}\frac{\partial u_3}{\partial \alpha_2}\right) + \frac{1}{A_1 A_2}\left(\frac{u_1}{R_1} - \frac{1}{A_1}\frac{\partial u_3}{\partial \alpha_1}\right)\frac{\partial A_2}{\partial \alpha_1}\right]\right\} \\ & + h_{36}\left\{\frac{1}{A_2}\frac{\partial u_1}{\partial \alpha_2} + \frac{1}{A_1}\frac{\partial u_2}{\partial \alpha_1} - \frac{u_1}{A_1 A_2}\frac{\partial A_1}{\partial \alpha_2} - \frac{u_2}{A_1 A_2}\frac{\partial A_2}{\partial \alpha_1}\right. \\ & + r_{12}^s\left[\frac{A_1}{A_2}\frac{\partial}{\partial \alpha_2}\left(\frac{u_1}{R_1} - \frac{1}{A_1}\frac{\partial u_3}{\partial \alpha_1}\right)\frac{1}{A_1} + \frac{A_2}{A_1}\frac{\partial}{\partial \alpha_1}\left(\frac{u_1}{R_1} - \frac{1}{A_1}\frac{\partial u_3}{\partial \alpha_1}\right)\frac{1}{A_1}\right. \\ & \left.\left.\left. - \frac{1}{A_1 A_2}\left(\frac{u_1}{R_1} - \frac{1}{A_1}\frac{\partial u_3}{\partial \alpha_1}\right)\frac{\partial A_1}{\partial \alpha_2} - \frac{1}{A_1 A_2}\left(\frac{u_2}{R_2} - \frac{1}{A_2}\frac{\partial u_3}{\partial \alpha_2}\right)\frac{\partial A_2}{\partial \alpha_1}\right]\right\}\right\} A_1 A_2\, \mathrm{d}\alpha_1\, \mathrm{d}\alpha_2. \end{aligned} \tag{11}$$

This signal equation is generic that can be simplified to account for many standard geometries, e.g., spherical shells, conical shells, paraboloidal shells, plates, etc., by using two Lamé parameters and two radii of curvature of the geometry [16].

3. Distributed sensing of linear conical shell

Application of the generic shell signal equation to specific geometries requires two Lamé parameters and two radii of curvature defined for the geometries. The Lamé parameters, radii of curvature, and principle directions of conical shells are, respectively, defined by $A_1 = 1$, $A_2 = x \sin \beta^*$, $R_1 = R_x = \infty$, $R_2 = R_\psi = x \tan \beta^*$, $\alpha_1 = x$, and $\alpha_2 = \psi$. Fig. 1 illustrates a conical shell and its parameters. Assume there is a distributed piezoelectric sensor layer laminated on the conical shell and the sensor layer is insensitive to the in-plane twisting S^s_{12}. The signal–strain relation of the distributed conical shell sensor layer becomes

$$\phi^s = \left(\frac{h^s}{S^e}\right) \int_x \int_\psi \left(h_{31} S^s_{xx} + h_{32} S^s_{\psi\psi}\right) x \sin \beta^* \, \mathrm{d}x \, \mathrm{d}\psi, \tag{12}$$

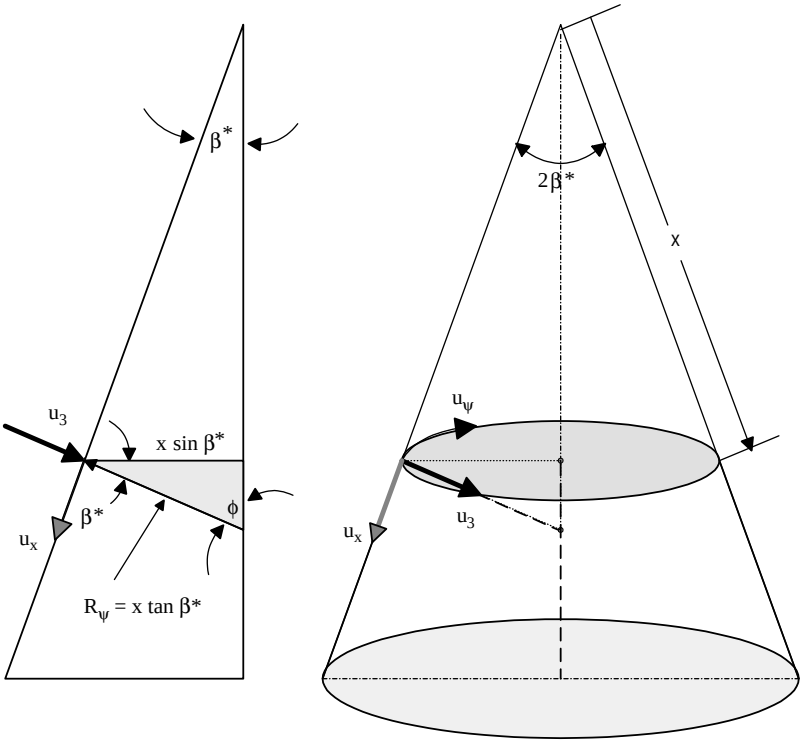

Fig. 1. Conical shell of revolution.

where the strain terms are $S^s_{xx} = s^o_{xx} + r^s_x k_{xx}$ and $S^s_{\psi\psi} = s^o_{\psi\psi} + r^s_\psi k_{\psi\psi}$. The membrane strain–displacement relations of the linear conical shell are

$$s^o_{xx} = \frac{\partial u_x}{\partial x} \quad \text{and} \quad s^o_{\psi\psi} = \frac{1}{x\sin\beta^*}\frac{\partial u_\psi}{\partial \psi} + \frac{u_x}{x} - \frac{u_3}{x\tan\beta^*}. \tag{13, 14}$$

According to the Donnel–Mushtari–Vlasov theory, the in-plane displacements u_x and u_ψ are usually neglected in the bending strains. Thus, the bending strains of the conical shell with the Donnel–Mushtari–Vlasov assumptions are

$$k_{xx} = -\frac{\partial^2 u_3}{\partial x^2} \quad \text{and} \quad k_{\psi\psi} = -\frac{1}{x^2\sin^2\beta^*}\frac{\partial^2 u_3}{\partial \psi^2} - \frac{1}{x}\frac{\partial u_3}{\partial x}. \tag{15, 16}$$

Substituting all strain–displacement relations into the sensing signal equation gives the signal–displacement expression of the generic distributed conical shell sensor,

$$\phi^s = \left(\frac{h^s}{S^e}\right)\int_x\int_\psi h_{31}\left\{\frac{\partial u_x}{\partial x} - r^s_x\frac{\partial^2 u_3}{\partial x^2}\right\} + h_{32}\left\{\frac{1}{x\sin\beta^*}\frac{\partial u_\psi}{\partial\psi} + \frac{u_x}{x} - \frac{u_3}{x\tan\beta^*} + r^s_\psi\left[-\frac{1}{x^2\sin^2\beta^*}\frac{\partial^2 u_3}{\partial\psi^2} - \frac{1}{x}\frac{\partial u_3}{\partial x}\right]\right\} x\sin\beta^*\,\mathrm{d}x\,\mathrm{d}\psi. \tag{17}$$

Note that this signal–displacement equation is only valid for linear conical shell sensors, since it does not involve any large deformation effect. Detailed modal contributions to the signal outputs of the distributed conical shell sensor are discussed next.

4. Modal voltages of conical shells

Distributed sensing characteristics are mode dependent. Distributed modal voltages and micro-signal generations of linear conical shells are discussed in this section. Consider a truncated conical shell section with free–free boundary conditions at the top and bottom perimeters and it is laminated with distributed piezoelectric sensor layers, Fig. 2. Thus, there is no shear force and moment at the free boundaries, i.e., at $x = x_1$ and x_2:

$$N_{xx} = N^*_{xx} = 0, \quad N_{x\psi} = N^*_{x\psi} = 0, \tag{18, 19}$$

$$\frac{1}{x}\left[\frac{\partial}{\partial x}(xM_{xx}) - M_{\psi\psi} - 2\frac{\partial M_{x\psi}}{\partial\psi}\csc\beta^*\right] = \frac{1}{x}\left[xQ^*_{xx} - \csc\beta^*\frac{\partial M^*_{x\psi}}{\partial\psi}\right] = 0, \tag{20}$$

$$M_{xx} = M^*_{xx} = 0. \tag{21}$$

The assumed modal displacement solutions for the free–free truncated conical shell of revolution are [3]

$$u_x = U_{xm}(x)\cos m\psi\sin\omega t,\ u_\psi = U_{\psi m}(x)\sin m\psi\sin\omega t,\ u_3 = U_{3m}(x)\cos m\psi\sin\omega t, \tag{22–24}$$

where m is the wave number and $m = 2\ldots\infty$, ω is the natural frequency, $U_{xm}(x)$, $U_{\psi m}(x)$ and $U_{3m}(x)$ are arbitrary displacement functions of x, satisfying the displacement boundary conditions. (Note that it is a rigid-body mode when $m = 1$.) $U_{xm}(x)\cos m\psi$ is the longitudinal

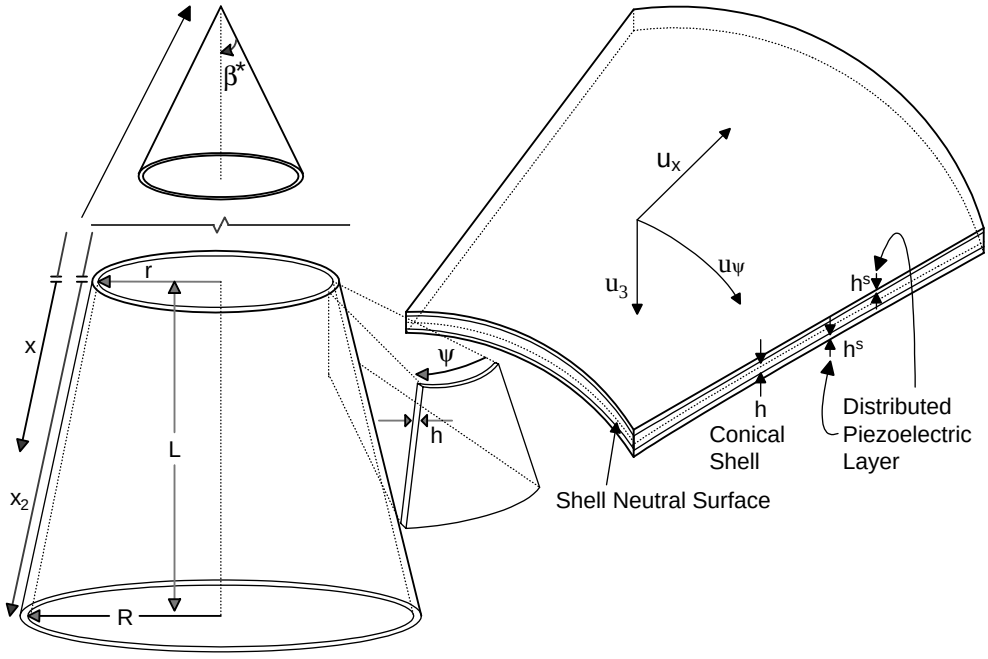

Fig. 2. Truncated conical shell section with free–free boundary conditions.

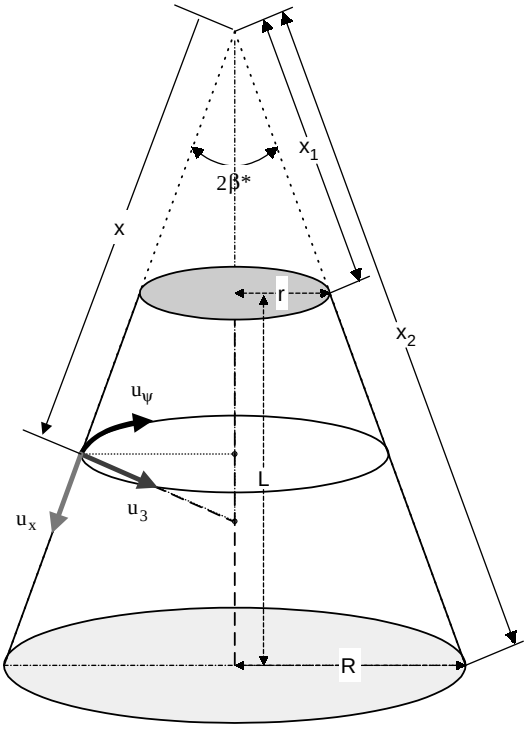

Fig. 3. Truncated conical shell section.

mode shape function, $U_{\psi m}(x)\sin m\psi$ is the circumferential mode shape function, and $U_{3m}(x)\cos m\psi$ is the transverse mode shape function within the Donnel–Mushtari–Vlasov theory. In free vibration analysis, the displacement function is chosen as $(x/x_2)^p$ defined in a polynomial form where "p" is the power of the polynomial function and x_2 is the (longitudinal) length from the apex to the bottom perimeter (Fig. 2). The polynomial form of displacement functions is chosen as to represent the flexibility of the shell structure in the longitudinal direction, since the structure is completely free. Higher-degree polynomial functions of $U_{xm}(x)$, $U_{\psi m}(x)$ and $U_{3m}(x)$ usually improve the analysis accuracy, especially for natural frequencies of higher circumferential modes. The generic micro-signal equation requires the spatial mode shape functions, not the

Table 1
Definitions of the two conical shell models

	Model 1	Model 2
Conical shell half-angle β^* (deg.)	14.24	30.24
Major radius, R (in)	6.07	7.95
Minor radius, r (in)	2.72	3.49
Length, L (in)	3.2	7.65
Thickness (in)	0.01	0.01

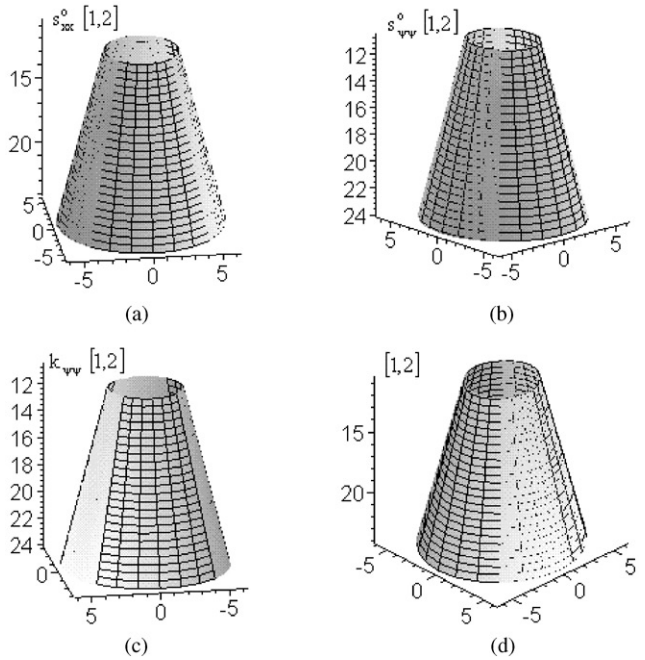

Fig. 4. Signal components and modal voltage of (1,2) mode, Model 1. (a) s^o_{xx}: the longitudinal membrane signal; (b) $s^o_{\psi\psi}$: the circumferential membrane signal; (c) $k_{\psi\psi}$: the circumferential bending signal; and (d) [1,2]: the (1,2)*th modal voltage*.

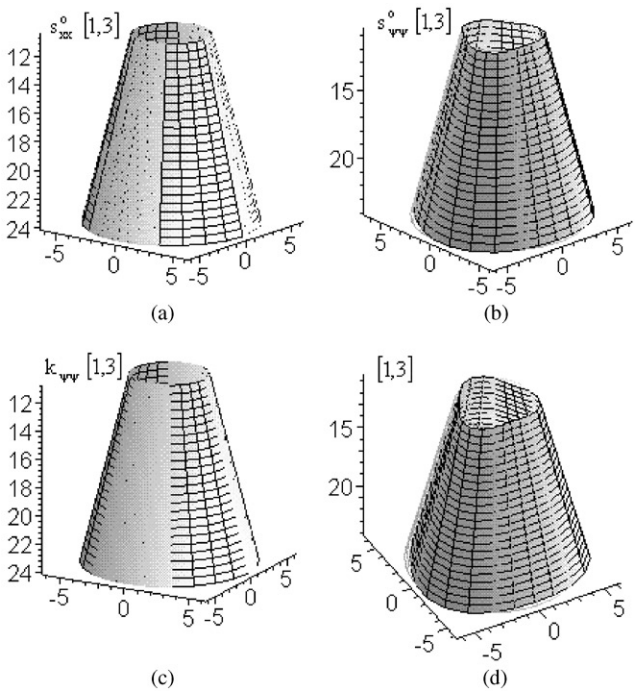

Fig. 5. Signal components and modal voltage of (1,3) mode, Model 1. (a) s^o_{xx}: the longitudinal membrane signal; (b) $s^o_{\psi\psi}$: the circumferential membrane signal; (c) $k_{\psi\psi}$: the circumferential bending signal; and (d) [1,3]: the (1,3)*th modal voltage*.

temporal part in the original displacement functions. Eliminating the temporal part and substituting three spatial mode shape functions into the sensing signal equation yields the mth modal signal expression $(\phi^s)_m$,

$$\phi^s = (\phi^s)_m = \left(\frac{h^s}{S^e}\right)\int_x\int_\psi \left\{h_{31}\left[\frac{\partial U_{xm}(x)\cos m\psi}{\partial x} + r^s_x\left(-\frac{\partial^2 U_{3m}(x)\cos m\psi}{\partial x^2}\right)\right]\right.$$
$$+ h_{32}\left[\frac{mU_{\psi m}(x)\cos m\psi}{x\sin\beta^*} + \frac{U_{xm}(x)\cos m\psi}{x} - \frac{U_{3m}(x)\cos m\psi}{x\tan\beta^*}\right.$$
$$\left.\left. + r^s_\psi\left(\frac{m^2 U_{3m}(x)\cos m\psi}{x^2\sin^2\beta^*} - \frac{1}{x}\frac{\partial U_{3m}(x)\cos m\psi}{\partial x}\right)\right]\right\} x\sin\beta^*\,\mathrm{d}x\,\mathrm{d}\psi. \tag{25}$$

Recall that $U_{xm}(x)$, $U_{\psi m}(x)$ and $U_{3m}(x)$ are defined as $(x/x_2)^p$. Choosing the modal function as $(x/x_2)^p$ with $p=1$ for the first-mode group $(1,m)$, substituting it into Eq. (25), and taking derivatives with respect to x, one can derive the modal sensing signal $(\phi^s)_m$ for the first mode group of linear conical shells,

$$\phi^s = (\phi^s)_m = \left(\frac{h^s}{S^e}\right)\int_x\int_\psi \left\{h_{31}\left(\frac{\cos m\psi}{x_2}\right) + h_{32}\left[\frac{m\cos m\psi}{x_2\sin\beta^*} + \frac{\cos m\psi}{x_2} - \frac{\cos m\psi}{x_2\tan\beta^*}\right.\right.$$
$$\left.\left. + r^s_\psi\left(\frac{m^2\cos m\psi}{xx_2\sin^2\beta^*} - \frac{1}{x}\frac{\cos m\psi}{x_2}\right)\right]\right\} x\sin\beta^*\,\mathrm{d}x\,\mathrm{d}\psi. \tag{26}$$

Again, note that the above (1,*m*)th modal signal equations of the first mode group, respectively, defined for the linear truncated conical shells were derived when $p=1$ in the displacement function $(x/x_2)^p$. When evaluating the (2,m)th modal signals (i.e., the second mode group) of the linear truncated conical shells, one needs to follow the same procedures using the displacement function $(x/x_2)^p$ with $p=2$ in the derivations, and so for the higher mode groups of linear conical shells,

$$\phi^s=(\phi^s)_m=\left(\frac{h^s}{S^e}\right)\int_x\int_\psi\left\{h_{31}\left(\frac{\cos m\psi}{x_2}+2\frac{x\cos m\psi}{x_2^2}-2r_x^s\left(\frac{\cos m\psi}{x_2^2}\right)\right)\right.$$
$$+h_{32}\left[\frac{\cos m\psi}{x_2}+\frac{x\cos m\psi}{x_2^2}-\left(\frac{\cos m\psi}{x_2}+\frac{x\cos m\psi}{x_2^2}\right)\cot\beta^*+\frac{m\cos m\psi}{x_2\sin\beta^*}+\frac{x\,m\cos m\psi}{x_2^2\sin\beta^*}\right.$$
$$\left.\left.+r_\psi^s\left(\frac{m^2\cos m\psi}{xx_2\sin^2\beta^*}+\frac{m^2\cos m\psi}{x_2^2\sin^2\beta^*}-\left(\frac{1}{x}\frac{\cos m\psi}{x_2}+2\frac{\cos m\psi}{x_2^2}\right)\right)\right]\right\}x\sin\beta^*\,\mathrm{d}x\,\mathrm{d}\psi. \quad (27)$$

Furthermore, note that the above signal equations represent the overall modal signal generation of the distributed sensor and then "averaged" over the effective sensor area S^e. Local microscopic signal magnitudes can be inferred only when the sensor area becomes infinitesimally small and the global average effect is neglected. Local micro-signal generations $(\phi^s)_m^*$ of the first two mode

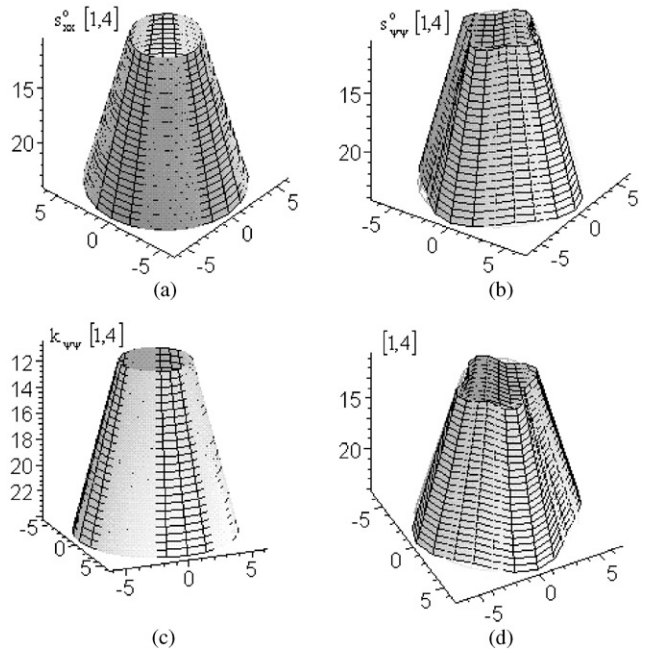

Fig. 6. Signal components and modal voltage of (1,4) mode, Model 1. (a) s_{xx}^o: the longitudinal membrane signal; (b) $s_{\psi\psi}^o$: the circumferential membrane signal; (c) $k_{\psi\psi}$: the circumferential bending signal; and (d) [1,4]: the (1,4)*th modal voltage*.

groups of conical shells are, respectively, represented as

$$\phi^s = (\phi^s)^*_m = h^s \left\{ h_{31} \left(\frac{\cos m\psi}{x_2} \right) + h_{32} \left[\frac{m \cos m\psi}{x_2 \sin \beta^*} + \frac{\cos m\psi}{x_2} - \frac{\cos m\psi}{x_2 \tan \beta^*} + r^s_\psi \left(\frac{m^2 \cos m\psi}{x x_2 \sin^2 \beta^*} - \frac{1}{x} \frac{\cos m\psi}{x_2} \right) \right] \right\}, \tag{28}$$

$$\phi^s = (\phi^s)^*_m = h^s \left\{ h_{31} \left(\frac{\cos m\psi}{x_2} + 2\frac{x \cos m\psi}{x_2^2} - 2r^s_x \left(\frac{\cos m\psi}{x_2^2} \right) \right) + h_{32} \left[\frac{\cos m\psi}{x_2} + \frac{x \cos m\psi}{x_2^2} - \left(\frac{\cos m\psi}{x_2} + \frac{x \cos m\psi}{x_2^2} \right) \cot \beta^* + \frac{m \cos m\psi}{x_2 \sin \beta^*} + \frac{x\, m \cos m\psi}{x_2^2 \sin \beta^*} + r^s_\psi \left(\frac{m^2 \cos m\psi}{x x_2 \sin^2 \beta^*} + \frac{m^2 \cos m\psi}{x_2^2 \sin^2 \beta^*} - \left(\frac{1}{x} \frac{\cos m\psi}{x_2} + 2\frac{\cos m\psi}{x_2^2} \right) \right) \right] \right\}. \tag{29}$$

Accordingly, detailed spatial distribution of local micro-signals (i.e., the distributed *modal voltages*) can be established and spatially distributed modal sensing characteristics can be studied.

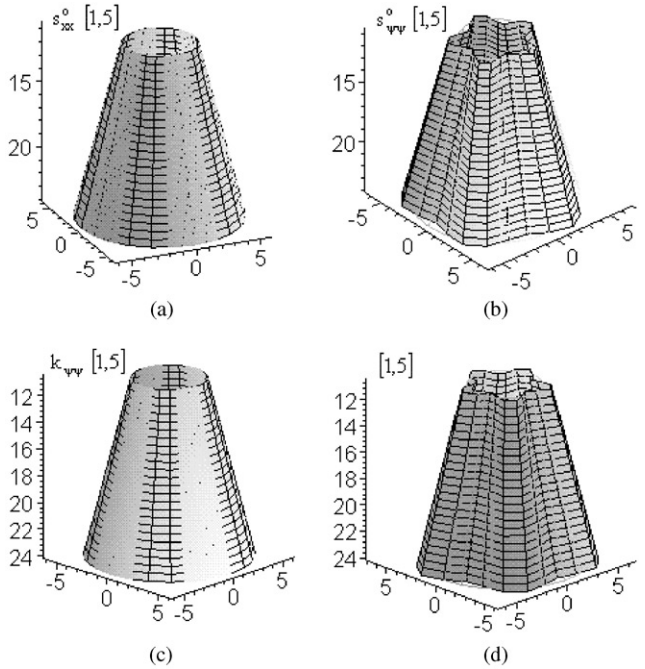

Fig. 7. Signal components and modal voltage of (1,5) mode, Model 1. (a) s^o_{xx}: the longitudinal membrane signal; (b) $s^o_{\psi\psi}$: the circumferential membrane signal; (c) $k_{\psi\psi}$: the circumferential bending signal; and (d) [1,5]: the (1,5)*th modal voltage*.

5. Evaluation of modal voltages and signal components

Distributed sensing signals and modal voltages of the conical shells of revolution were defined above. Modal signals and micro-signal components of two models of truncated conical shell section are studied, Fig. 3. Both models have the same thickness, however, the apex angle and length of the second model are larger than the first model, i.e., 30.24° versus 14.24° and 7.65 in versus 3.2 in. Accordingly, natural frequencies of the second model are lower than those of the first model [3]. This frequency variation would also influence the signal generation of various modal voltages. Dimensions and geometrical parameters of

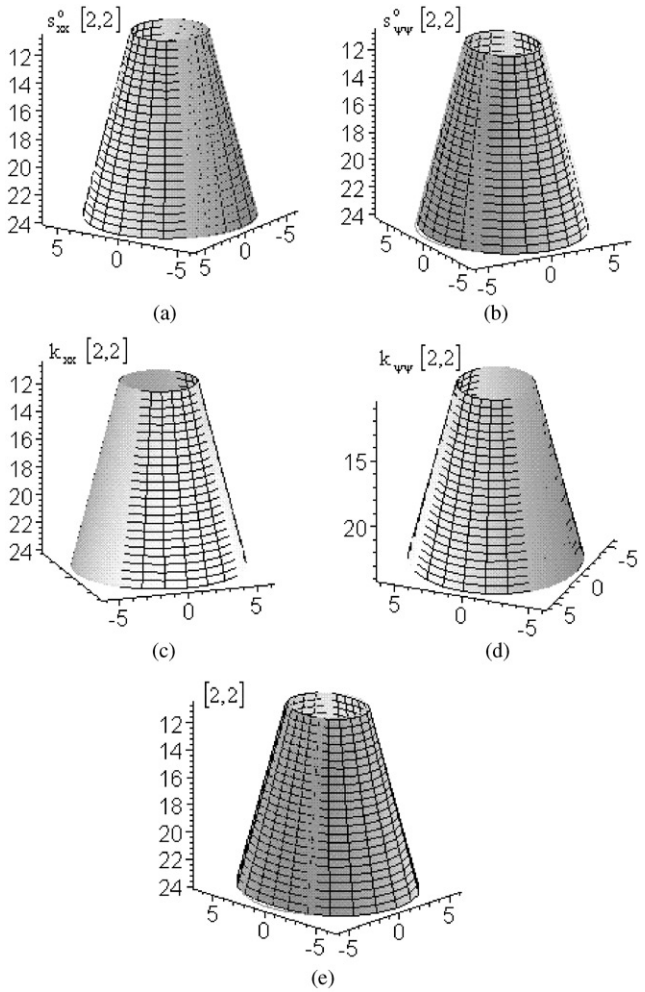

Fig. 8. Signal components and modal voltage of (2,2) mode, Model 1. (a) s^o_{xx}: the longitudinal membrane signal; (b) $s^o_{\psi\psi}$: the circumferential membrane signal; (c) k_{xx}: the longitudinal bending signal; $k_{\psi\psi}$: the circumferential bending signal; and (d) [2,2]: the (2,2)*th modal voltage*.

the two conical shells are summarized in Table 1. Four modal voltage distributions and micro-signal generations of two mode groups (i.e., the first and the second groups with $m=2$, 3, 4, 5) of two conical shells are presented first, followed by observations and discussions in this section.

Recall that the in-plane displacements u_x and u_ψ are neglected in the bending strains but not in the membrane strains, based on the Donnel–Mushtari–Vlasov theory, so the mode shape functions were defined based on the theory. Detailed micro-signal contributions from the membrane and bending strain components are evaluated, so the significant signal component(s) can be identified and appropriate design guidelines can be inferred. Also, note that the $m=1$ mode of conical shell with free boundary conditions is the rigid body motion. The shell rigid body

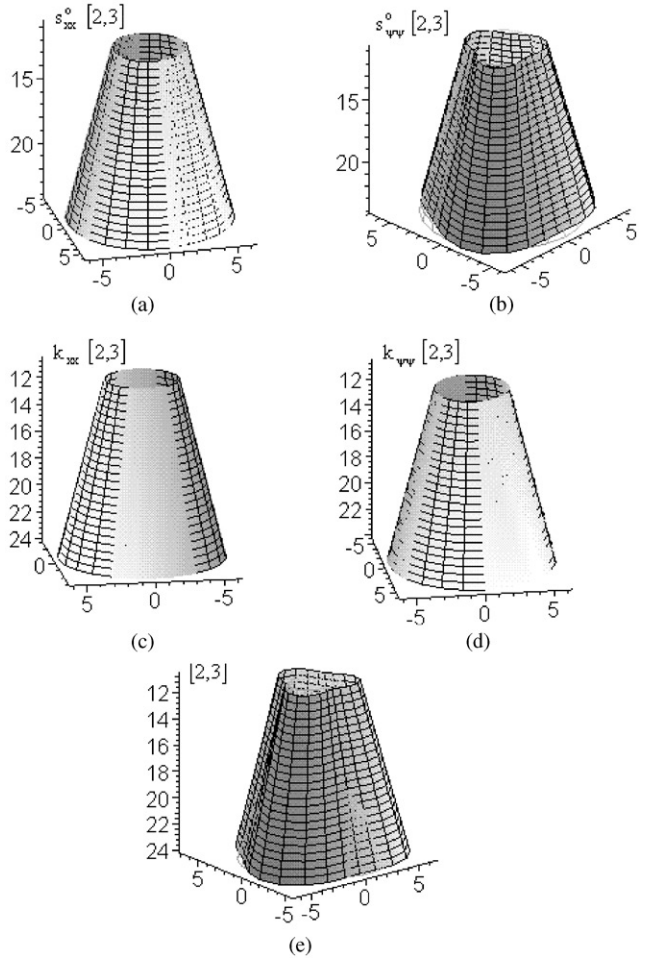

Fig. 9. Signal components and modal voltage of (2,3) mode, Model 1. (a) s^o_{xx}: the longitudinal membrane signal; (b) $s^o_{\psi\psi}$: the circumferential membrane signal; (c) k_{xx}: the longitudinal bending signal; (d) $k_{\psi\psi}$: the circumferential bending signal; and (e) [2,3]: the (2,3)*th modal voltage*.

mode ($m = 1$) contributes no signal generation. Thus, micro-signals and modal voltages of natural modes with $m \geq 2$ are investigated in case studies.

5.1. Model 1, the first mode group (1, $m = 2-5$)

Distributed modal voltages and signal components of the first mode group (1, $m = 2-5$) of Model-1 are presented in Figs. 4–7. The top-left signal distribution denotes the signal component resulting from the longitudinal membrane strain, the top-right signal denotes the signal component resulting from the circumferential membrane strain, the bottom-left signal denotes the signal component resulting from the circumferential bending strain, and the bottom-right denotes the overall signal distribution—*the (k,m)th modal voltage*, including all contributing

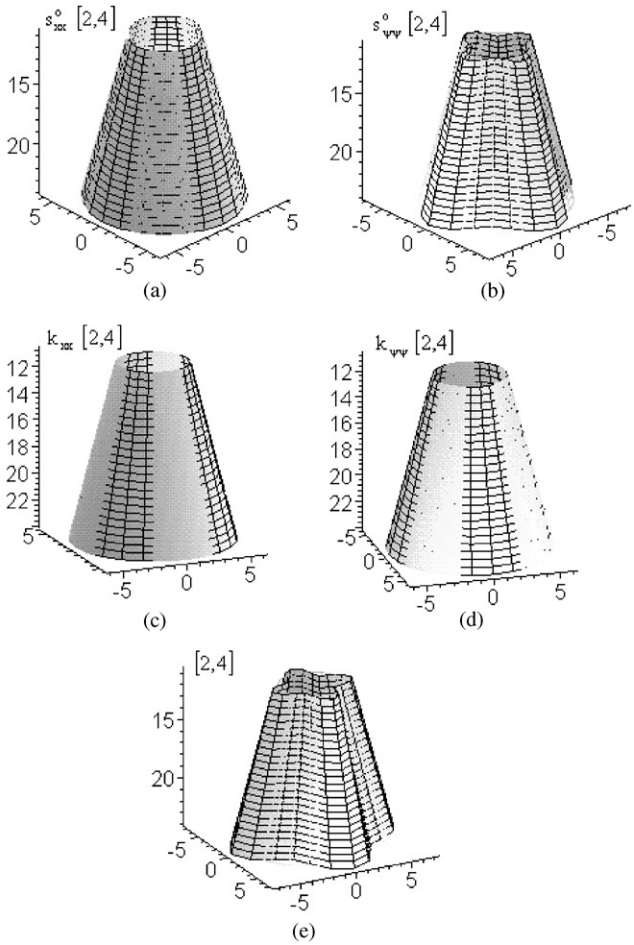

Fig. 10. Signal components and modal voltage of (2,4) mode, Model 1. (a) s^o_{xx}: the longitudinal membrane signal; (b) $s^o_{\psi\psi}$: the circumferential membrane signal; (c) k_{xx}: the longitudinal bending signal; (d) $k_{\psi\psi}$: the circumferential bending signal; and (e) [2,4]: the (2,4)*th modal voltage*.

micro-signal components. Note that the longitudinal bending strain signal vanishes due to the selected displacement function with $p = 1$.

5.2. Model 1, the second mode group (2, $m = 2-5$)

Distributed modal voltages and micro-signal components of the second mode group (2, $m = 2-5$) of Model 1 are presented in Figs. 8–11. The top-left signal distribution denotes the signal component resulting from the longitudinal membrane strain, the top-right signal denotes the signal component resulting from the circumferential membrane strain, the middle-left signal

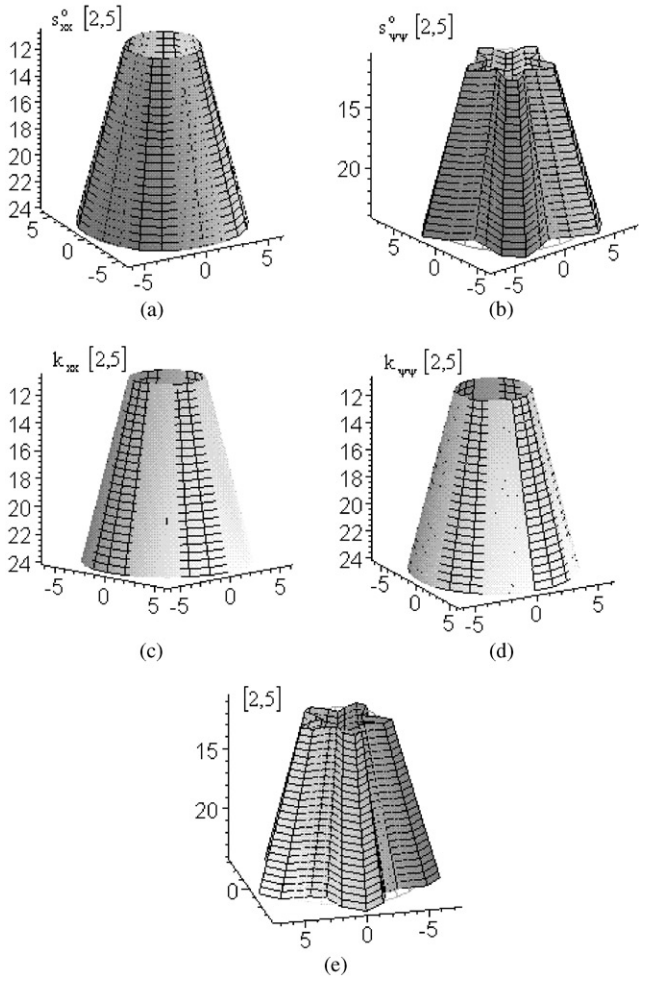

Fig. 11. Signal components and modal voltage of (2,5) mode, Model 1. (a) s^o_{xx}: the longitudinal membrane signal; (b) $s^o_{\psi\psi}$: the circumferential membrane signal; (c) k_{xx}: the longitudinal bending signal; (d) $k_{\psi\psi}$: the circumferential bending signal; and (e) [2,5]: the (2,5)*th modal voltage*.

denotes the signal component resulting from the longitudinal bending strain, the middle-right signal denotes the signal component resulting from the circumferential bending strain, and the bottom-left denotes the overall signal distribution—*the (k,m)th modal voltage*, including all contributing signal components. Note that the longitudinal bending strain exists in this case, with the displacement function $p = 2$.

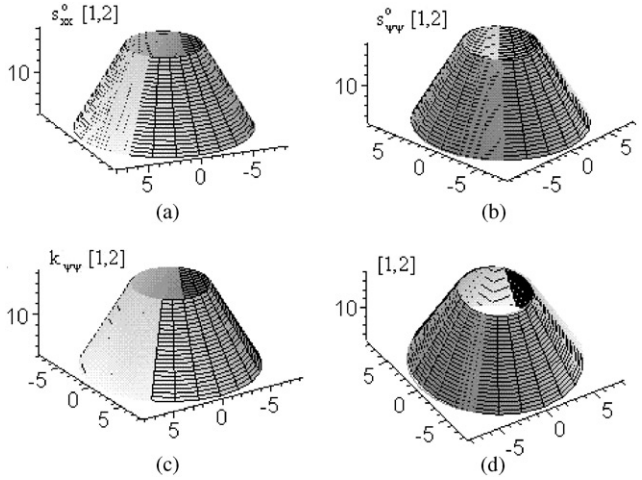

Fig. 12. Signal components and modal voltage of (1,2) mode, Model 2. (a) s^o_{xx}: the longitudinal membrane signal; (b) $s^o_{\psi\psi}$: the circumferential membrane signal; (c) $k_{\psi\psi}$: the circumferential bending signal; and (d) [1,2]: the (1,2)*th modal voltage*.

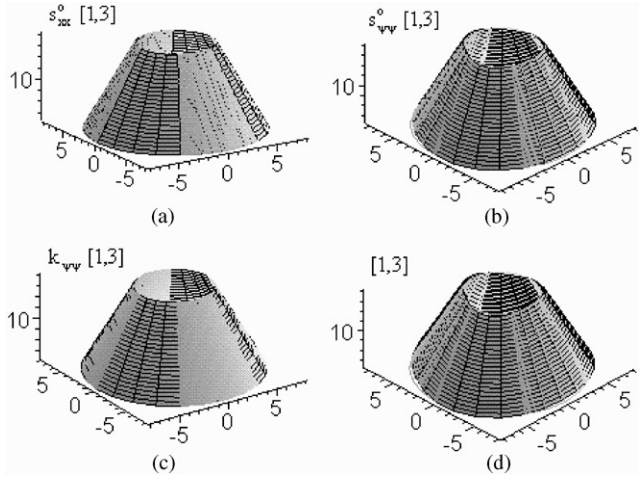

Fig. 13. Signal components and modal voltage of (1,3) mode, Model 2. (a) s^o_{xx}: the longitudinal membrane signal; (b) $s^o_{\psi\psi}$: the circumferential membrane signal; (c) $k_{\psi\psi}$: the circumferential bending signal; and (d) [1,3]: the (1,3)*th modal voltage*.

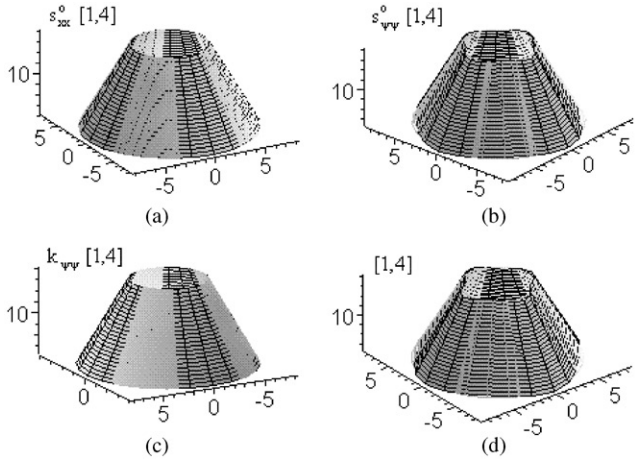

Fig. 14. Signal components and modal voltage of (1,4) mode, Model 2. (a) s^o_{xx}: the longitudinal membrane signal; (b) $s^o_{\psi\psi}$: the circumferential membrane signal; (c) $k_{\psi\psi}$: the circumferential bending signal; and (d) [1,4]: the (1,4)*th modal voltage*.

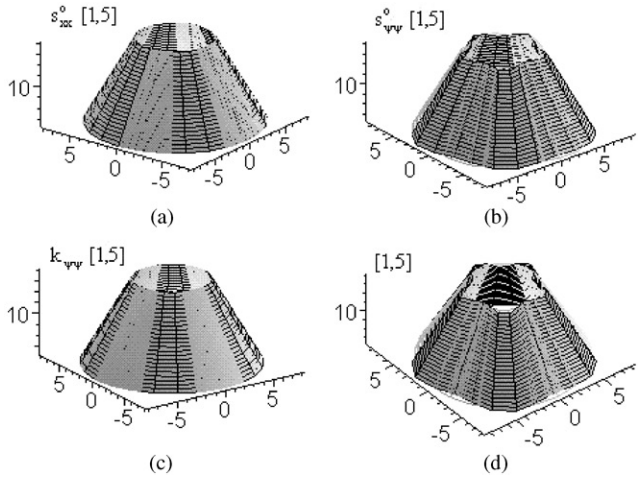

Fig. 15. Signal components and modal voltage of (1,5) mode, Model 2. (a) s^o_{xx}: the longitudinal membrane signal; (b) $s^o_{\psi\psi}$: the circumferential membrane signal; (c) $k_{\psi\psi}$: the circumferential bending signal; and (d) [1,5]: the (1,5)*th modal voltage*.

5.3. *Model 2, the first mode group (1, m = 2−5)*

Distributed modal voltages and micro-signal components of the first mode group (1, $m = 2-5$) of Model 2 are presented in Figs. 12–15. Arrangements of the signal components are the same as those of the first mode group of Model 1. The final signal distribution—*the (k,m)th*

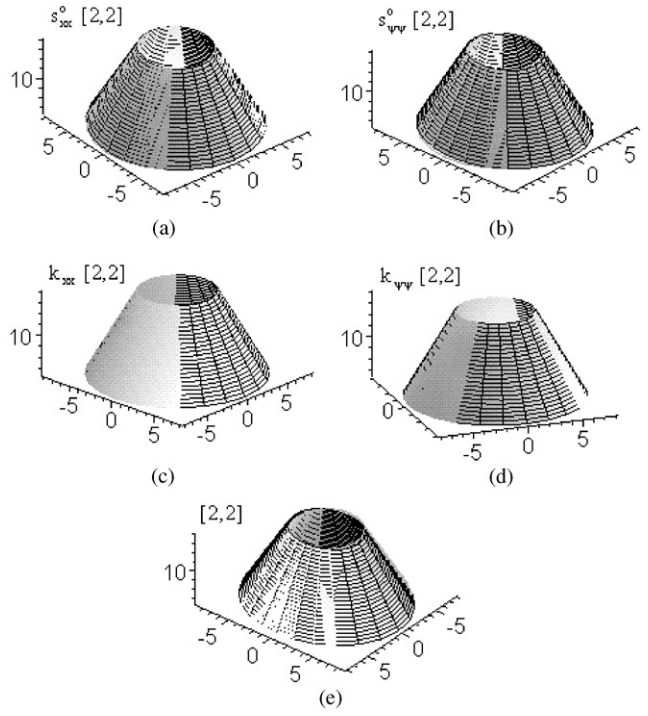

Fig. 16. Signal components and modal voltage of (2,2) mode, Model 2. (a) s^o_{xx}: the longitudinal membrane signal; (b) $s^o_{\psi\psi}$: the circumferential membrane signal; (c) k_{xx}: the longitudinal bending signal; (d) $k_{\psi\psi}$: the circumferential bending signal; and (e) [2,2]: the (2,2)*th modal voltage*.

modal voltage, including all contributing signal components, is the bottom-right plot. Again, the longitudinal bending strain vanishes due to the selected displacement function with $p = 1$.

5.4. *Model 2, the second mode group (2, $m = 2-5$)*

Distributed modal voltages and micro-signal components of the second mode group (2, $m = 2-5$) of Model 2 are presented in Figs. 16–19. Arrangements of component plots are similar to the second mode group of Model 1. The bottom-left signal distribution denotes *the (k,m)th modal voltage*, including all contributing signal components. Note that the longitudinal bending strain exists due to the selected displacement function with $p = 2$.

Observing these modal voltages and comparing their micro-signal components of two conical shell models suggests that the dominating signal component among the four signal components (i.e., the longitudinal membrane component, the circumferential membrane component, the longitudinal bending component, and the circumferential bending component) is the circumferential membrane component. This circumferential component dominates the signal generation for lower shell modes and/or deep shells (i.e., Model 2). Usually, high strain regions result in high signal magnitudes. Accordingly, the spatially distributed signal patterns—*the modal*

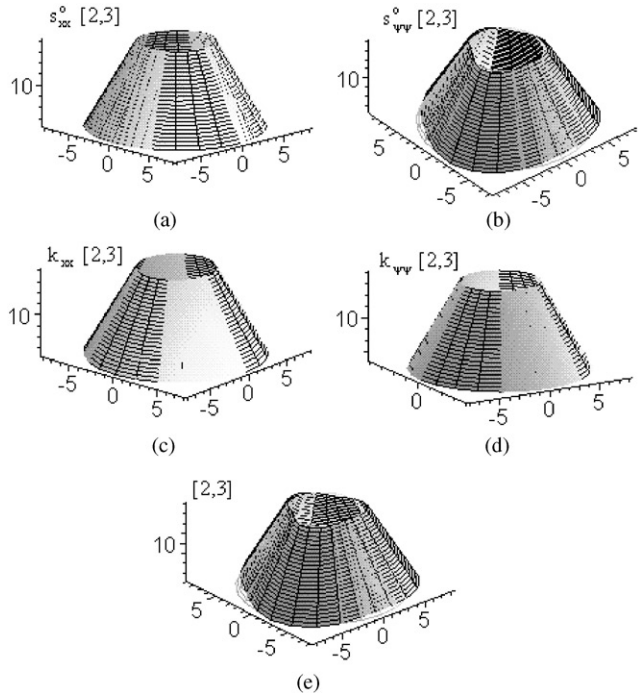

Fig. 17. Signal components and modal voltage of (2,3) mode, Model 2. (a) s^o_{xx}: the longitudinal membrane signal; (b) $s^o_{\psi\psi}$: the circumferential membrane signal; (c) k_{xx}: the longitudinal bending signal; (d) $k_{\psi\psi}$: the circumferential bending signal; and (e) [2,3]: the (2,3)*th modal voltage*.

voltages—clearly reveal the distinct modal dynamic and micro-strain characteristics of conical shells.

6. Conclusions

Conical shell structures and components are often used as nozzles, injectors, blades, rocket fairings, etc., in turbomachinery, aerospace structures, micro-electromechanical systems, etc. This study is to investigate the dynamic sensing characteristics, micro-signal generations, and distributed modal voltages of truncated conical shell sections.

Spatially distributed sensing signals of a distributed piezoelectric sensor layer laminated on a generic double-curvature elastic shell were discussed first. The generic sensing signal equation was derived based on the direct piezoelectric effect, the Gauss theory, the open-circuit assumption, the Maxwell equation, and also the generic double-curvature thin shell theory. Microscopic signal components contributed from various meridional and circumferential membrane/bending strain components were evaluated and the final signal–displacement equation was defined and applied to conical shells using two Lamé parameters and two radii of curvature defined for the conical shell geometry. With the Donnel–Mushtari–Valsov theory, the final closed-form sensing signal expression was defined based on given boundary conditions and mode

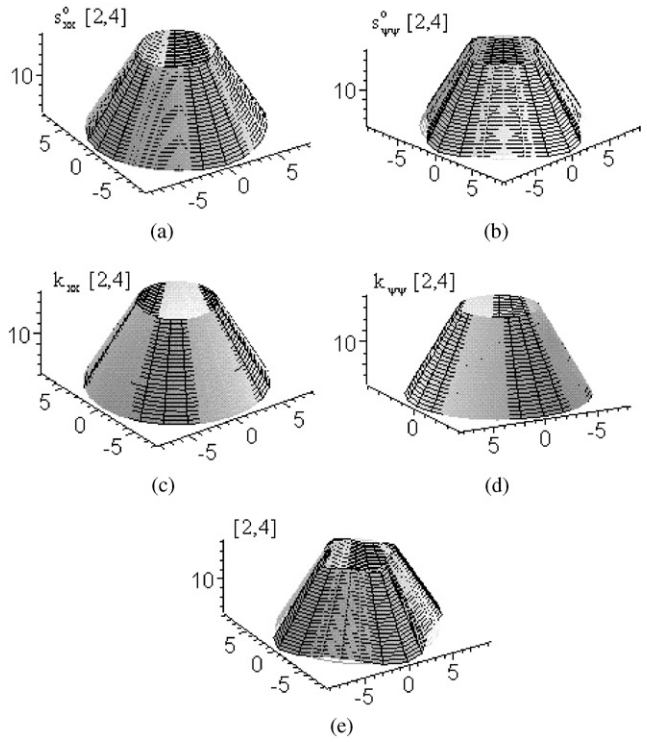

Fig. 18. Signal components and modal voltage of (2,4) mode, Model 2. (a) s^o_{xx}: the longitudinal membrane signal; (b) $s^o_{\psi\psi}$: the circumferential membrane signal; (c) k_{xx}: the longitudinal bending signal; (d) $k_{\psi\psi}$: the circumferential bending signal; and (e) [2,4]: the (2,4)*th modal voltage*.

shape functions. The assumed mode shape functions have a polynomial expression $(x/x_2)^p$ for the longitudinal waves and trigonometric (sine or cosine) expression for the circumferential waves.

Distributed signal components and modal voltages of two truncated conical shells with the same thickness and different shell apex angles and sizes were evaluated. Two mode groups and four modal signals of the two conical shell models were calculated and plotted. Distributed modal voltages and their various signal components of the two conical shell models reveal that the dominating signal component among the four contributing micro-signal components (i.e., the longitudinal membrane component, the circumferential membrane component, the longitudinal bending component, and the circumferential bending component) is the circumferential membrane component. This circumferential component is even more dominating for lower shell modes and/or deep shells. In general, high strain regions result in high signal magnitudes. Accordingly, the spatially distributed signal patterns—*the modal voltages*—clearly represent the modal dynamic and strain characteristics of conical shells. Spatially distributed micro-signals also reveal critical regions showing significant or minimal signal magnitudes. Appropriate selection of regional signal components can further enhance the distributed control effectiveness of conical shells.

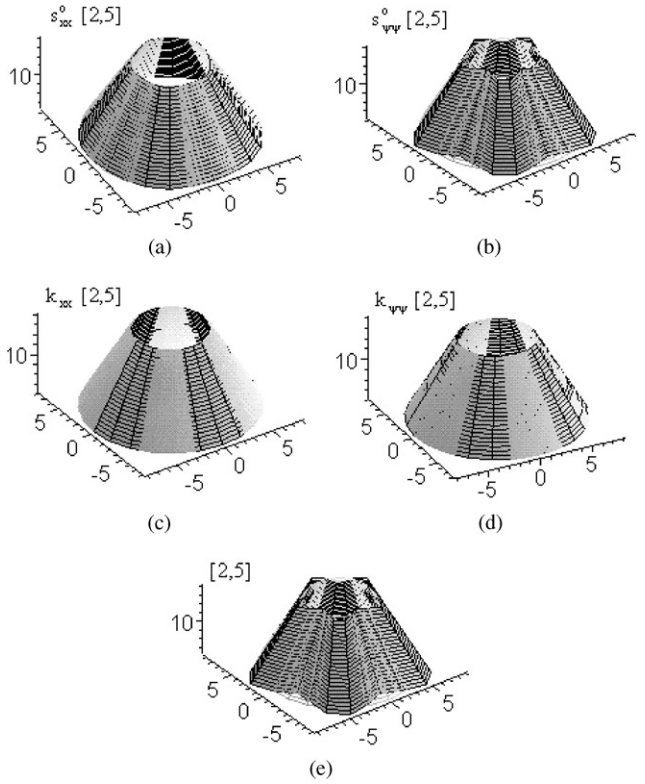

Fig. 19. Signal components and modal voltage of (2,5) mode, Model 2. (a) s^o_{xx}: the longitudinal membrane signal; (b) $s^o_{\psi\psi}$: the circumferential membrane signal; (c) k_{xx}: the longitudinal bending signal; (d) $k_{\psi\psi}$: the circumferential bending signal; and (e) [2,5]: the (2,5)*th modal voltage*.

Acknowledgements

This research is supported, in part, by a grant (F49620–98–1-0467) from the Air Force Office of Scientific Research (Project Manager: Brian Sanders). This support is gratefully acknowledged.

References

[1] W.C.L. Hu, J.F. Gormley, U.S. Lindholm, Flexural vibrations of conical shells with free edges, NASA Report CR 384, 1966.
[2] R.A. Newton, Free vibrations of rocket nozzles, American Institute Aeronatics and Astonautics Journal 4 (1966) 1303–1305.
[3] F.A. Krause, Natural Frequencies and Mode Shapes of the Truncated Conical Shell with Free Edges, Ph.D. Dissertation, The University of Arizona, Tucson, (1968).
[4] V.G. Bazhenov, V. Igonicheva, Nonlinear analysis of nonaxisymmetric buckling of cylindrical and conical shells in axial impact, Prikladnaya Mekhanika 23 (1987) 10–17.

[5] Y. Kobayashi, G. Yamada, K.I. Harada, Unstable vibration of a spinning truncated conical shell, Transaction of the Japan Society of Mechanical Engineers 56 (1990) 1347–1351.
[6] B. Wang, C.W.S. To, Vibration analysis of truncated conical thin shell structures, Journal of Sound and Vibration 150 (1991) 509–516.
[7] K.M. Liew, M.K. Lim, C.W. Lim, D.B. Li, Y.R. Zhang, Effects of initial twist and thickness variation on the vibration behaviour of shallow conical shells, Journal of Sound and Vibration 180 (1995) 271–296.
[8] C.W. Lim, K.M. Liew, Vibration of shallow conical shells with shear flexibility: a first order theory, International Journal of Solids Structures 33 (1996) 451–468.
[9] V.D. Souza, J.M.F. Saraiva, Analysis of free vibrations of conical shells using Donnell's approximations, American Society of Mechanical Engineers, Applied Mechanics 48 (1995) 84–89.
[10] L. Tong, Effect of axial load on free vibration of orthotropic truncated conical shells, Transaction of the American Society of Mechanical Engineers, Journal of Vibration & Acoustics 118 (1996) 164–168.
[11] H.S. Tzou, D.W. Wang, Dynamics and distributed control of conical shells laminated with full and diagonal actuators, Journal of Sound and Vibration 256 (2002) 65–79.
[12] U. Gabbert, H.S. Tzou (Eds.), Smart Structures and Structronic Systems, Kluwer Academic Publishers, Dordrecht, 2001.
[13] H.S. Tzou, G.L. Anderson (Eds.), Intelligent Structural Systems, Kluwer Academic Publishers, Dordrecht, 1992.
[14] R. Howard, W.K. Chai, H.S. Tzou, Modal voltages of linear and nonlinear structures using distributed artificial neurons, Mechanical Systems and Signal Processing 15 (2001) 629–640.
[15] H.S. Tzou, Thin–layer distributed piezoelectric neurons and muscles: electromechanics and applications, in: H.S. Tzou, T. Fukuda (Eds.), Precision Sensors, Actuators, and Systems, Kluwer Academic Publishers, Dordrecht, 1992 pp 175–218.
[16] H.S. Tzou, Piezoelectric Shells-Distributed Sensing and Control of Continua, Kluwer Academic Publishers, Dordrecht, 1993.
[17] H.S. Tzou, R.J. Yang, Nonlinear piezo-thermoelastic shell theory applied to control of variable-geometry shells, Journal of Theoretical and Applied Mechanics 38 (2000) 623–644.